Received: 10 February 2022 | Revised: 22 March 2022 | Accepted: 2 April 2022

DOI: 10.1002/asl.1093

RESEARCH ARTICLE

Atmospheric Science Letters RMetS

# The opposite response of the South Asian high to increasing $CO_2$ at different heights

**Xia Qu**[1,2] | **Gang Huang**[2,3,4] | **Hongyu Hou**[2,4] | **Zesheng Chen**[5] | **Yan Du**[5,6,7]

[1]Center for Monsoon System Research, Institute of Atmospheric Physics, Chinese Academy of Sciences, Beijing, China

[2]State Key Laboratory of Numerical Modeling for Atmospheric Sciences and Geophysical Fluid Dynamics, Institute of Atmospheric Physics, Chinese Academy of Sciences, Beijing, China

[3]Laboratory for Regional Oceanography and Numerical Modeling, Qingdao National Laboratory for Marine Science and Technology, Qingdao, China

[4]University of Chinese Academy of Sciences, Beijing, China

[5]State Key Laboratory of Tropical Oceanography, South China Sea Institute of Oceanology, Chinese Academy of Sciences, Guangzhou, China

[6]College of Marine Science, University of Chinese Academy of Sciences, Beijing, China

[7]Southern Marine Science and Engineering Guangdong Laboratory, Guangzhou, China

**Correspondence**

Xia Qu, Center for Monsoon System Research, Institute of Atmospheric Physics, Chinese Academy of Sciences, Beijing, China; State Key Laboratory of Numerical Modeling for Atmospheric Sciences and Geophysical Fluid Dynamics, Institute of Atmospheric Physics, Chinese Academy of Sciences Beijing, China. P. O. Box 9804, Beijing 100029, China.

Email: quxia@mail.iap.ac.cn

**Funding information**

Chinese Academy of Sciences, Grant/Award Number: COMS2019Q03; Ministry of Science and Technology of the People's Republic of China, Grant/Award Number: 2019QZKK0102; National Natural Science Foundation of China, Grant/Award Numbers: 41831175, 42175055, LTO2005, XDA20060501; National Key Scientific and Technological Infrastructure project "Earth System Science Numerical Simulator Facility" (EarthLab)

## Abstract

Based on the multimodel ensemble of 22 models in Coupled Model Intercomparison Project Phase 6 (CMIP6), the present manuscript found that in response to increasing $CO_2$, the South Asian high (SAH) displays the opposite response over its southern region in the upper troposphere: an anticyclonic response at 100 hPa and a weak (insignificant) cyclonic response at 200 hPa. This opposite response is a product of tropospheric warming. In response to increasing $CO_2$, the troposphere warms, with the potential temperatures peaking at 150–200 hPa over the northern Indian Ocean (IO). With transportation by local vertical motion (ascendance over the northeastern IO and descendance over the northwestern IO), various changes in vertical temperature advection with height form at 100 and 200 hPa. Finally, the changes contribute to a decrease in the $\omega$ response with pressures at 100 hPa but an increase in the $\omega$ response with pressures at 200 hPa over the northwestern IO. Over the northwestern IO, $\omega$ change is inversely related to pressure. At 100 hPa, the sign of $\omega$ changes with pressure, which yields distinct vorticity forcing over the northeastern and northwestern IO. This causes an anticyclonic response, which may generate zonal vorticity advection and balance the vorticity forcing. At 200 hPa, the contribution is roughly opposite to that at 100 hPa. In addition, although diabatic heating contributes to the vertical profile of $\omega$, it yields the same-sign vorticity response at 100 and 200 hPa.

KEYWORDS

increasing $CO_2$, South Asian high, vertical response

## 1 | INTRODUCTION

The South Asian high (SAH; also called the South Asian monsoon anticyclone) is a zonally-elongate anticyclone in the upper troposphere and lower stratosphere during the boreal summer (Figure 1a,b). It stretches zonally from North Africa to the North Pacific and longitudinally spans from the equator to approximately 50°N. Its center resides over South Asia and the Tibetan Plateau. It forms mainly due to the topographic heating of the Tibetan Plateau and the latent heating released by South Asian monsoon rainfall (Boos & Kuang, 2010; Flohn, 1960; Wu et al., 2012). The southern component of the SAH is the tropical easterlies, which are tightly associated with underlying tropical storms (Rao et al., 2008); the northern component, the Asian subtropical westerlies, is an important environmental factor that forces downstream rainfall (Kosaka et al., 2011; Liang & Wang, 1998; Sampe & Xie, 2010). In addition, the SAH is strongly coupled with the underlying convection, which forms a pathway for the transport of pollutants emitted at the surface to the upper troposphere and lower stratosphere and affects the vertical distribution of these pollutants (Bian et al., 2020; Park et al., 2009).

Since the mid-19th century, the concentration of carbon dioxide ($CO_2$) in the atmosphere has been increasing, leading to profound influences on the climate (Stocker et al., 2013). However, the SAH responses to increasing $CO_2$ are height-dependent (Qu et al., 2015; Qu & Huang, 2016). Figure 1e,f display the responses of horizontal wind and vorticity to $CO_2$ increases at 100 hPa and 200 hPa, respectively. At 100 hPa, the tropical component of the anticyclone is enhanced, and its center generally moves southwards (Figure 1e); meanwhile, at 200 hPa, the component displays a weak opposite-sign vorticity response (Figure 1f). In previous studies on the SAH, circulation changes at a single level were frequently used to quantify SAH changes, especially the variability on interannual timescales (Huang et al., 2011; Wei et al., 2015; Zhang et al., 2002). However, the current understanding implies that under global warming, it is insufficient to quantify the SAH change based on circulation at a single pressure level and that one should be aware of how its responses differ with height.

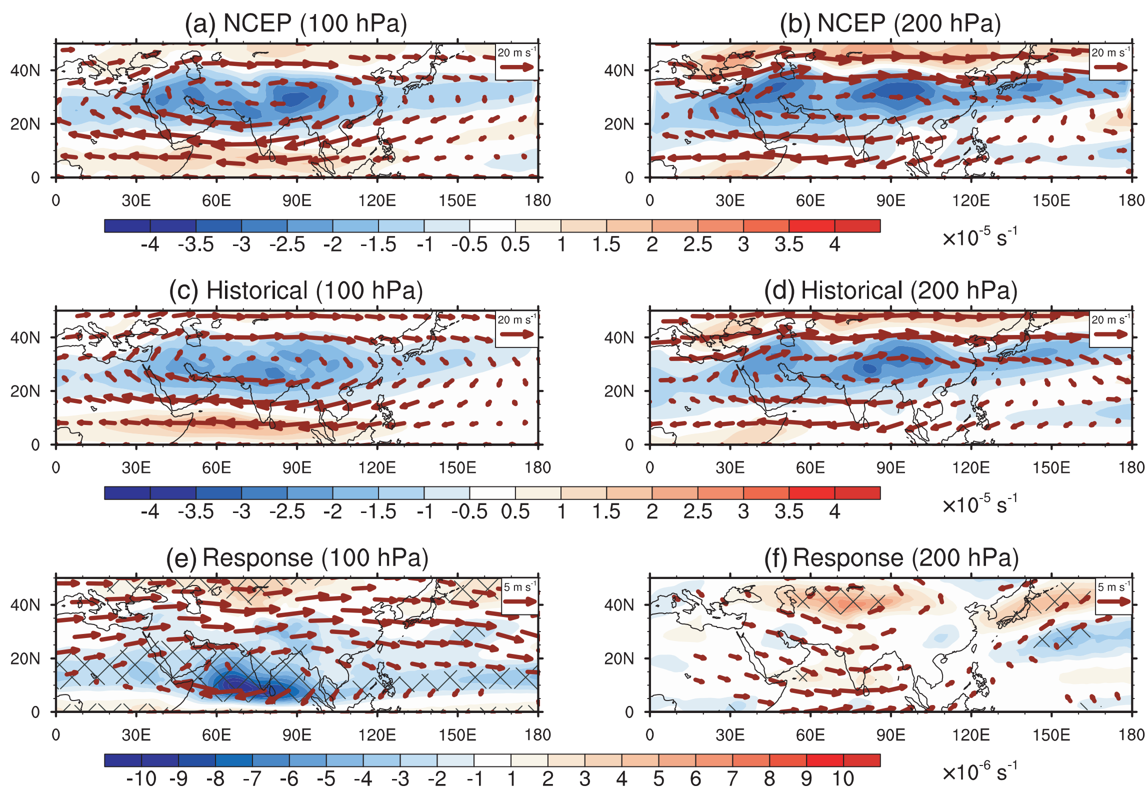


FIGURE 1 The June–august climatology (a–d) and responses (e and f) of horizontal wind (vectors) and vorticity (color shading; unit: $S^{-1}$) in the upper troposphere. The left column shows the results at 100 hPa, and the right column shows the results at 200 hPa. (a and b) The climatological results of the NCEP reanalysis; (c and d) the climatological results of the CMIP6 MME in the historical experiment. The climatology is the average during 1980–2010. (e and f) The responses in the CMIP6 1%$CO_2$ experiment (the response is the difference in climatology between years 121–140 and years 1–20). The lattice patterns indicate that the response of vorticity reaches the 95% significance level; in (e and f), only vectors at the 95% significance level are displayed. All the results are multimodel ensemble results

The above contrary responses in the upper troposphere indicate that the SAH undergoes an elevation change during an increase in $CO_2$. Simultaneously, some other climate phenomena also display similar responses. For instance, as $CO_2$ increases, the global atmosphere warms, leading to the rising of the tropopause elevation (Hu & Vallis, 2019; Santer et al., 2003); as tropical convective anvil clouds form at a relatively fixed temperature, the height of high clouds rises in response to global warming (Hartmann & Larson, 2002). Correspondingly, tropical convection deepens; for instance, in climatological ascendance regions, the ascendance is enhanced in the upper troposphere but weakens in the mid- and lower-troposphere (Chou et al., 2009). Among these phenomena, the SAH response seems to be one component of the troposphere deepening under global warming.

In addition, the tropical troposphere warms in response to $CO_2$-induced global warming, with a maximum temperature increase in the upper troposphere (Ma et al., 2012); over the IO sector, the warming maximum resides at approximately 200 hPa (Knutson & Manabe, 1995). This may lead to different stratification effects in the vertical direction. Does it affect the contrary responses of the SAH in the upper troposphere? The rest of this paper attempts to address the above question.

# 2 | DATA AND METHODS

## 2.1 | Data and model performances

The present study used the monthly outputs of 22 models in CMIP6 (Eyring et al., 2016), the information of which is provided in Table S1. The experiments used were (1) 1% $CO_2$ experiments (the $CO_2$ concentration in the models increased 1% per year until the concentration had quadrupled) and (2) historical experiments (observed forcings, such as anthropogenic and natural forcings, from the mid-19th century to 2014 were used to force the models). The present study used only the "r1i1p1f1" runs in each model. The multimodel ensemble (MME) method was used to assess the overall performance and sequential response of the models. The data were interpolated onto a 1.0° × 1.0° grid.

To evaluate the model performance, the following observational and reanalysis data were used: (1) the Global Precipitation Climatology Project (GPCP) monthly precipitation analysis (Adler et al., 2003) and (2) the NCEP reanalysis (Kalnay et al., 1996). When evaluating the model performance, we focused on the period from 1980 to 2010 in the historical simulations, observational data and reanalysis data. Evaluation shows that the CMIP6 MME reasonably reproduces the climatology of the upper-tropospheric circulation, temperature and the rainfall associated with the SAH (Figures 1a–d, S1a,b and S2a,b).

The response to increasing $CO_2$ was defined to be the difference in climatology between years 121–140 and years 1–20 in the 1% $CO_2$ experiments. The significance level of the response (Figure 1e,f) is based on Student's *t* test, performed furtherly based on the intermodel standard deviation of climatologies of years 121–140 and years 1–20, respectively. The significance level of diagnostic results (Figure 2) is based on the confidence interval. For a grid, if the values in confidence interval of the diagnostic results of all the models do not contain 0, the diagnostic result is significant.

## 2.2 | The diagnostic methods

The SAH featured a prominent vorticity, so the vorticity budget was diagnosed. Under increasing $CO_2$, the linearized equation of the vorticity budget is written as follows:

$$f\frac{\partial \omega'}{\partial p} - \overline{V}\cdot\nabla\zeta' - V\cdot\overline{\zeta} - \beta v' = 0 \tag{1}$$

where the overbars and primes represent climatology and response, respectively. $f$, $\omega$, $V$, $\zeta$, $\beta$, and $v$ are the Coriolis parameter, pressure velocity, horizontal wind, vorticity, and variation in the Coriolis parameter with latitude and meridional wind, respectively. The first term on the right-hand side of Equation (1) is vorticity forcing.

Thermodynamic processes may contribute to changes in vertical motion. Thus, the associated diagnosis is employed. Its linearized equation is written as follows:

$$C_\mathrm{p}\left[(V\cdot\nabla \mathrm{T})' + \left(\frac{p}{p_0}\right)^k\left(\omega'\frac{\partial\overline{\theta}}{\partial p} + \overline{\omega}\frac{\partial\theta'}{\partial p}\right)\right] = Q_1 \tag{2}$$

where $C_\mathrm{p}$, $T$, $p$, $\theta$ and $Q_1$ represent the specific heat at constant pressure, temperature, pressure, potential temperature and diabatic heating, respectively. $k = R/C_\mathrm{p}$. $p_0$ = 1000 hpa.

Assuming $B = \left(\frac{p}{p_0}\right)^k$, then:

$$(V\cdot\nabla \mathrm{T})' + B\left(\omega'\frac{\partial\overline{\theta}}{\partial p} + \overline{\omega}\frac{\partial\theta'}{\partial p}\right) = \frac{Q_1}{C_\mathrm{p}} \tag{3}$$

Then:

$$\omega' = \frac{Q_1}{BC_\mathrm{p}\frac{\partial\overline{\theta}}{\partial p}} - \frac{\overline{\omega}}{\frac{\partial\overline{\theta}}{\partial p}}\frac{\partial\theta'}{\partial p} - \frac{(V\cdot\nabla \mathrm{T})'}{B\frac{\partial\overline{\theta}}{\partial p}} \tag{4}$$

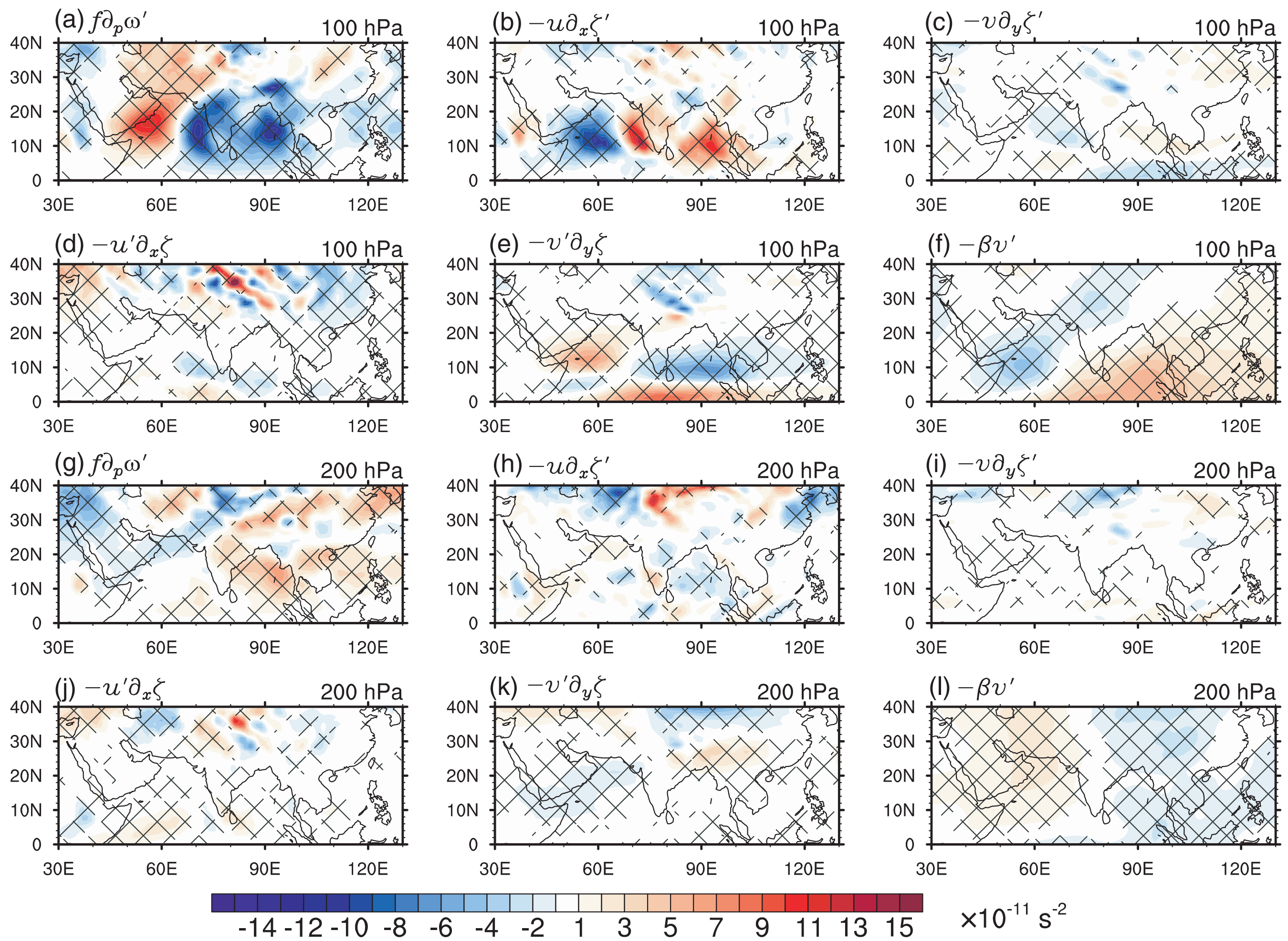


**FIGURE 2** The terms (color shading) of the vorticity budget (based on Equation (1)) at 100 hPa (a–f) and 200 hPa (g–l). The units are $s^{-2}$. The lattice patterns indicate the terms reaching the 95% significance level

For convenience, we named the first to third terms on the right-hand side of Equation (4) the contributions of diabatic heating, stratification and horizontal temperature advection, respectively.

## 3 | RESULTS

As displayed in Section 1, the SAH is a large anticyclone mainly located over subtropical Asia, with its latitude spanning from the equator to approximately 50°N (Figure 1a,b); in the CMIP6 MME results, the SAH displayed the same features (Figure 1c,d). In response to increasing $CO_2$, the behaviors of the SAH are roughly reversed south of 30°N in the upper troposphere (Figure 1e,f). At 100 hPa, there is an intensified anticyclonic response, with its maximum over the northern IO. It corresponds to a southward movement of the SAH. At 200 hPa, from 20° to 100°E, responses of significant westerlies and weak cyclones are found. These nearly divergent responses indicate an elevation of the SAH.

To understand the vorticity response associated with the SAH, we diagnosed the vorticity budget. Figure 2 displays the terms of Equation (1) at 100 and 200 hPa. The advection terms are divided into advection in zonal and meridional directions. The equation is mainly balanced by two terms: $f\frac{\partial\omega'}{\partial p}$ and $\left(-u\frac{\partial\zeta'}{\partial p}\right)$ (Figure 2a,b,g,h). At 100 hPa, the vorticity response, where it is transported by climatological westerlies, yields positive vorticity advection east of 70°E and negative advection west of 70°E (Figure 2b). This advection is generally offset by the effect of divergence change or the response of vertical motion with height $\left(f\frac{\partial\omega'}{\partial p}\right)$ (Figure 2a). That is, in response to increasing $CO_2$, at 100 hPa east of 70°E, $\omega'$ decreases with pressure. It favors the vorticity degeneration (Figure 2a). To balance the degeneration, a negative vorticity response occurs over the northern IO, with a maximum near 70°E (Figure 1e). With the transportation of climatological westerlies, positive vorticity advection exists east of 70°E, offsetting the vorticity degeneration led by the change in pressure velocity with height (Figure 2b). At 100 hPa west of 70°E, the processes are opposite (Figures 1e and 2a,b). The 100 hPa forms a steady vorticity response structure over the northern IO, and thus, the anomalous anticyclone is maintained. At 200 hPa over the northeastern IO, the responses are roughly opposite to those at 100 hPa (Figures 1f and 2g,h). Thus, the vertical velocity response with height leads to the opposite change in the SAH at 100 hPa and 200 hPa.

The contribution of the thermodynamic processes to the pressure velocity change was also investigated. Figure 3 displays the $\omega$ response of the CMIP6 MME, the response of diagnosed $\omega$ and the contribution of the terms in Equation (4). The $\omega$ response (as well as its variation with height) calculated based on Equation (4) is close to that of the CMIP6 MME (Figure 3a,b,f,g), indicating that the $\omega$ response to increasing $CO_2$ is likely the result of changes in diabatic heating, vertical temperature advection (stratification effect) and horizontal temperature advection.

Over the northeastern IO [5°–25°N, 70°–100°E], the ascendance features an enhancement in the upper troposphere, with a maximum at 150 hPa (Figure 3a). The $\omega$ response decreases with pressure at 100 hPa and increases with pressure at 200 hPa. This overall profile of the $\omega$ response is mainly led by the competing effects of diabatic heating and stratification (Figure 3b,c,d). To measure the difference in the $\omega$ response with pressure (hereafter DWP), we defined it as follows:

$$\mathrm{DWP} = \left(\frac{\partial \omega'}{\partial p}\right)_{100\,\mathrm{hPa}} - \left(\frac{\partial \omega'}{\partial p}\right)_{200\,\mathrm{hPa}} \tag{5}$$

The DWP of direct output of CMIP6 MME is $-1.5 \times 10^{-6}$ $s^{-1}$. The DWP of diagnosed $\omega'$, based on Equation (4), is $-1.1 \times 10^{-6}$ $s^{-1}$. The DWPs contributed by diabatic heating, stratification and horizontal temperature advection are $2.1 \times 10^{-6}$ $s^{-1}$, $-1.9 \times 10^{-6}$ $s^{-1}$, and $-0.5 \times 10^{-6}$ $s^{-1}$, respectively (Figure 3c,d,e). Thus, in the upper troposphere, the difference in the $\omega$ response with height (pressure) over the northeastern IO is mostly contributed by the stratification effect.

The impact of global warming on the tropics results in oceanic warming and moist adiabatic adjustment, leading to tropospheric warming (Knutson & Manabe, 1995; Ma et al., 2012). The associated potential temperature peaks

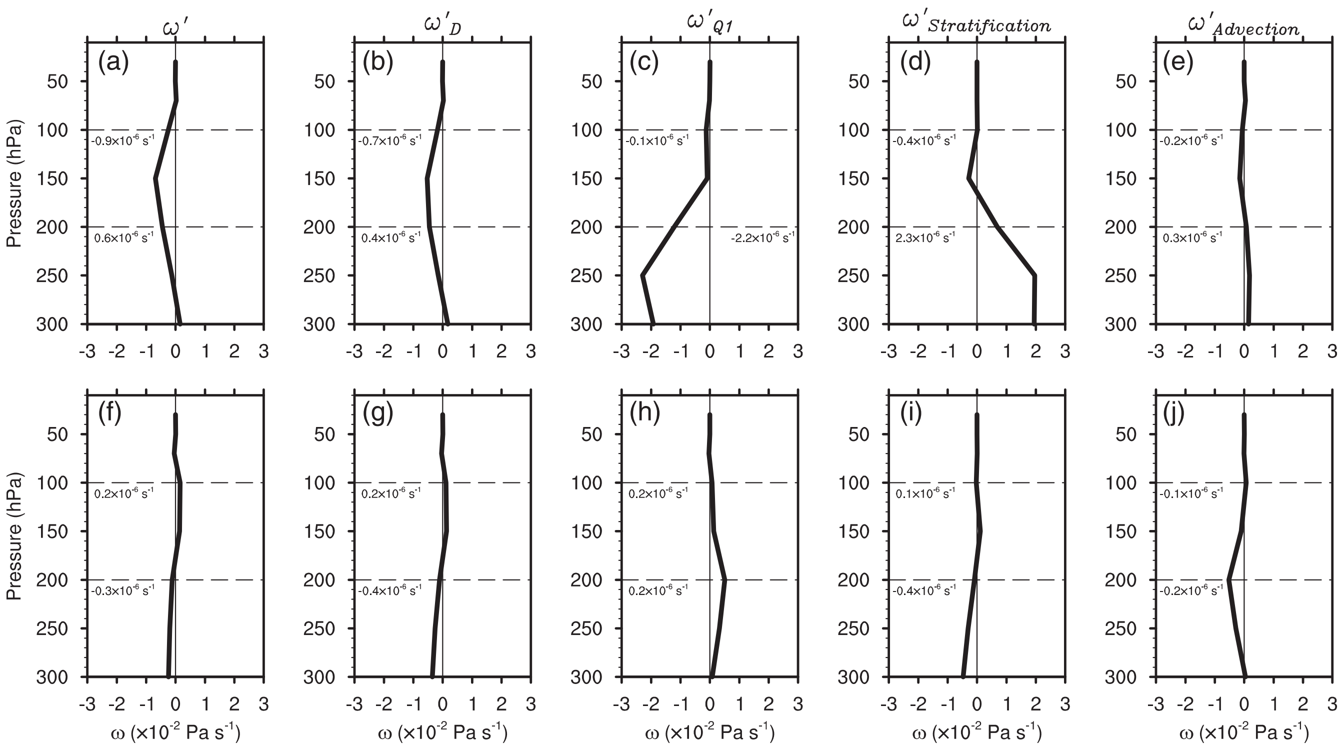


**FIGURE 3** The area-averaged response of $\omega$ (unit: Pa $s^{-1}$) with height. (a and f) The results of the model output. (b and g) The results of diagnosed $\omega$, based on Equation (4). (c and h) The $\omega$ responses due to diabatic heating. (d and i) The $\omega$ responses due to stratification. (c and h) The $\omega$ responses due to changes in horizontal temperature advection. The top row (a–e) is the result over the area [5°–25°N, 70°–100°E], and the bottom row (f–j) is the result over the area [5°–25°N, 50°–60°E]. The values are the results of $\frac{\partial \omega'}{\partial p}$ at the pressure level of the dashed lines

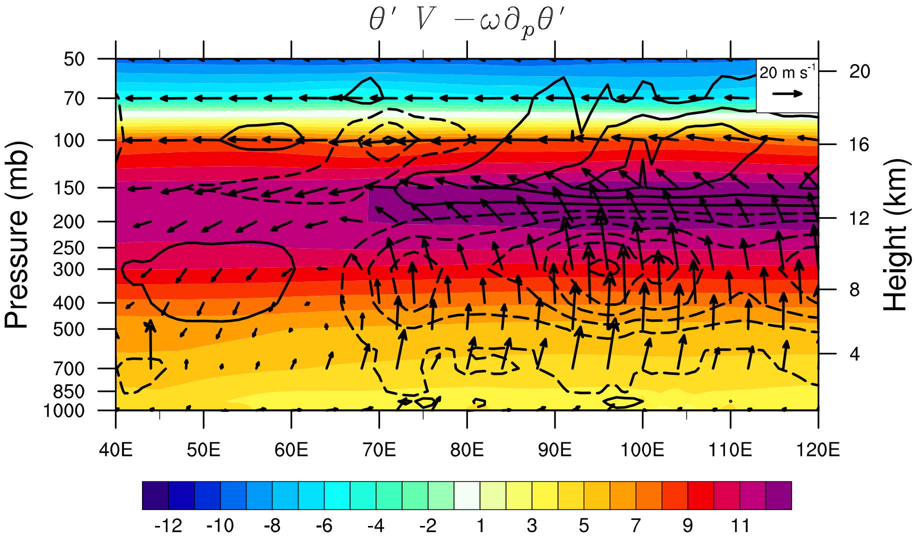


**FIGURE 4** The response of potential temperature (color shading, unit: K), climatological wind (vectors) and anomalous potential temperature transported by climatological vertical motion (contours, unit: K s$^{-1}$). The results are the average between 5° and 25°N. only contours for $\pm 0.2 \times 10^{-5}$, $\pm 0.6 \times 10^{-5}$, $\pm 1.0 \times 10^{-5}$, $\pm 1.4 \times 10^{-5}$, $\pm 1.8 \times 10^{-5}$, and $\pm$ $2.2 \times 10^{-5}$ K s$^{-1}$ are displayed. When displaying the vectors, the pressure velocity is multiplied by −500 for clarity

at 150–200 hPa over the northeastern IO (Figure 4). This leads to different stratification patterns at 100 hPa and 200 hPa. The climatologically local ascendance causes warm vertical advection at and above 150 hPa but cold vertical advection at and below 200 hPa (Figure 4). At and above 150 hPa, the warm advection leads to a compensation of upwards motion. As heights of 70 and 100 hPa are near the tropopause, the ascendance is weaker than that at 150 hPa. This leads to weaker warm vertical advection and thus a weakened compensation of upwards motion. The $\omega$ response with pressure is negative. At and below 200 hPa, the magnitude of cold vertical advection increases with pressure, which leads to the $\omega$ response with pressure being positive. Thus, the stratification effect induces a different $\omega$ response with pressure (height) over the northeastern IO.

Over the northwestern IO [5°–25°N, 50°–60°E], the descendance features an intensification at 100–150 hPa and a decline at and below 200 hPa (Figure 3f). This profile of $\omega$ response with height (pressure) is the competing effects of the diabatic heating, stratification effect and horizontal temperature advection (Figure 3h,i,j). The DWP of the direct output of CMIP6 MME is $0.5 \times 10^{-6}$ s$^{-1}$. That based on Equation (4) is $0.6 \times 10^{-6}$ s$^{-1}$. The DWPs contributed by diabatic heating, stratification and horizontal temperature advection are 0 s$^{-1}$, $0.5 \times 10^{-6}$ s$^{-1}$, and $0.1 \times 10^{-6}$ s$^{-1}$, respectively (Figure 3h,i,j). Thus, over the northwestern IO, the difference in the $\omega$ response with height (pressure) is also the contribution of the stratification effect.

In response to increasing $CO_2$, the potential temperature associated with tropospheric warming peaks at 150–200 hPa over the northwestern IO (Figure 4). This leads to a distinction in vertical temperature advection at 100 and 200 hPa. The climatologically local descendance causes warm vertical advection at 100 and 250 hPa but cold vertical advection at 150 hPa (Figure 4). As the climatological vertical motion is weak at 70 hPa, the vertical temperature advection is miniscule. Correspondingly, an anomalous contribution of upwards motion occurs at 100 and 250 hPa, an anomalous contribution of downwards motion occurs at 150 hPa, and a nonsignificant contribution of vertical motion takes place at 70 hPa. According to the centered finite difference, the $\omega$ response with pressure is positive at 100 hPa and negative at 200 hPa. Thus, similar to the situation over the northeastern IO, the stratification effect also leads to a different $\omega$ response with pressure (height) over the northwestern IO.

## 4 | SUMMARY AND DISCUSSION

Using the historical CMIP6 experiment, we found that the CMIP6 MME is capable of reproducing the climatology of the SAH and the underlying rainfall during summer (June–August). Therefore, the present study has focused mainly on the SAH changes during summer.

The output of the 1% $CO_2$ experiment suggests that, in response to increasing $CO_2$, the SAH behaves oppositely south of 30°N in the upper troposphere: at 100 hPa, there is an intensified anticyclonic response, with its maximum over the northern IO; at 200 hPa, from 20° to 100°E, responses of significant westerlies and weak cyclones are found. This nearly opposite response suggests an elevation rise of the SAH.

The vorticity budget suggests that over the northern IO at 100 and 200 hPa, the major terms are as follows: (1) the climatological vorticity transported by zonal wind and (2) the vertical gradient of anomalous pressure velocity ($\omega$) multiplied by the Coriolis parameter ($f$). These two terms generally cancel each other out. This result indicates that the vorticity change is the result of changes in the $\omega$ response with height (pressure).

Further diagnosis shows that the vertical profile of the changes in $\omega$ is mainly the result of diabatic heating and the stratification effect. Among these two contributors, the former leads to the same sign contribution to the changes in $\omega$ with height (pressure), while the latter mainly leads to the opposite-sign $\omega$ change with height (pressure).

The stratification effect, or the changes in temperature transported by climatological vertical motion, is mainly the result of tropospheric warming. The response to increasing $CO_2$ in the tropics results in oceanic warming and moist adiabatic adjustment, which lead to tropospheric warming. The associated potential temperature peaks at 150–200 hPa. Over the northeastern IO, the climatological ascendance peaks in the mid-troposphere and vanishes near 100 hPa. It interacts with changes in potential temperature and finally contributes to a decrease in the $\omega$ response with pressure at 100 hPa but an increase in the $\omega$ response with pressure at 200 hPa. In contrast, over the northwestern IO, the above atmosphere is dominated by descendance. Finally, the interaction of changes in potential temperature with the descendance results in an increase in the $\omega$ response with pressure at 100 hPa but a decrease in the $\omega$ response with pressure at 200 hPa.

The above results provide some implications for the changes under global warming. First, the changes in the upper troposphere may be nonuniform. In previous studies, circulation changes at a single level were frequently used to represent changes in upper/mid- troposphere, especially the variability on interannual timescales (Huang et al., 2011; Wei et al., 2015; Zhang et al., 2002). Present study implies that multilevel changes, rather than single-level changes, should be considered. Second, one should be aware of the height changes of some climatic phenomena. Especially under global warming, the increased height of tropopause may lead to the elevation of other climatic phenomenas. Finally, the stratification effect is also crucial under global warming, at least when studying the changes in the upper troposphere.

## ACKNOWLEDGEMENTS

We acknowledge the World Climate Research Programme, which, through its Working Group on Coupled Modeling, coordinated and promoted CMIP6. We thank the climate modeling groups for producing and making available their model output, the Earth System Grid Federation (ESGF) for archiving the data and providing access, and the multiple funding agencies who support CMIP6 and ESGF. The study was supported by the National Natural Science Foundation of China (NSFC; 41831175), Key Deployment Project of Centre for Ocean Mega-Research of Science, Chinese Academy of Sciences (COMS2019Q03), the NSFC (42175055), the Second Tibetan Plateau Scientific Expedition and Research (STEP) Program (2019QZKK0102), the Strategic Priority Research Program of the Chinese Academy of Sciences (XDA20060501), State Key Laboratory of Tropical Oceanography, South China Sea Institute of Oceanology, Chinese Academy of Sciences (Project No. LTO2005).

## AUTHOR CONTRIBUTIONS

**Xia Qu:** Conceptualization; data curation; formal analysis; funding acquisition; investigation; methodology; software; supervision; validation; visualization; writing – original draft; writing – review and editing. **Gang Huang:** Funding acquisition; project administration; supervision; writing – review and editing. **Hongyu Hou:** Software; writing – review and editing. **Zesheng Chen:** Funding acquisition; writing – review and editing. **Yan Du:** Funding acquisition; writing – review and editing.

## ORCID

*Xia Qu* https://orcid.org/0000-0003-2674-0472

## REFERENCES

Adler, R.F., Huffman, G.J., Chang, A., Ferraro, R., Xie, p.P., Janowiak, J. et al. (2003) The version-2 global precipitation climatology project (GPCP) monthly precipitation analysis (1979-present). *Journal of Hydrometeorology*, 4, 1147–1167.

Bian, J., Li, D., Bai, Z., Li, Q., Lyu, D. & Zhou, X. (2020) Transport of Asian surface pollutants to the global stratosphere from the Tibetan plateau region during the Asian summer monsoon. *National Science Review*, 7, 516–533.

Boos, W.R. & Kuang, Z. (2010) Dominant control of the south Asian monsoon by orographic insulation versus plateau heating. *Nature*, 463, 218–222.

Chou, C., Neelin, J.D., Chen, C.-A. & Tu, J.-Y. (2009) Evaluating the "rich-get-richer" mechanism in tropical precipitation change under global warming. *Journal of Climate*, 22, 1982–2005.

Eyring, V., Bony, S., Meehl, G.A., Senior, C.A., Stevens, B., Stouffer, R.J. et al. (2016) Overview of the coupled model Intercomparison project phase 6 (CMIP6) experimental design and organization. *Geoscientific Model Development*, 9, 1937–1958.

Flohn, H. (1960) Recent investigations on the mechanism of the "summer monsoon" of southern and eastern Asia. In: *Symposium on Monsoons of the World*. New Delhi: Hind Union Press, pp. 75–88.

Hartmann, D.L. & Larson, K. (2002) An important constraint on tropical cloud - climate feedback. *Geophysical Research Letters*, 29, 12-1–12-4.

Hu, S.N. & Vallis, G.K. (2019) Meridional structure and future changes of tropopause height and temperature. *Quarterly Journal of the Royal Meteorological Society*, 145, 2698–2717.

Huang, G., Qu, X. & Hu, K.M. (2011) The impact of the tropical Indian Ocean on south Asian high in boreal summer. *Advances in Atmospheric Sciences*, 28, 421–432.

Kalnay, E., Kanamitsu, M., Kistler, R., Collins, W., Deaven, D., Gandin, L. et al. (1996) The NCEP/NCAR 40-year reanalysis project. *Bulletin of the American Meteorological Society*, 77, 437–471.

Knutson, T.R. & Manabe, S. (1995) Time-mean response over the tropical Pacific to increased $CO_2$ in a coupled ocean-atmosphere model. *Journal of Climate*, 8, 2181–2199.

Kosaka, Y., Xie, S.P. & Nakamura, H. (2011) Dynamics of interannual variability in summer precipitation over East Asia. *Journal of Climate*, 24, 5435–5453.

Liang, X.Z. & Wang, W.C. (1998) Associations between China monsoon rainfall and tropospheric jets. *Quarterly Journal of the Royal Meteorological Society*, 124, 2597–2623.

Ma, J., Xie, S.P. & Kosaka, Y. (2012) Mechanisms for tropical tropospheric circulation change in response to global warming. *Journal of Climate*, 25, 2979–2994.

Park, M., Randel, W.J., Emmons, L.K. & Livesey, N.J. (2009) Transport pathways of carbon monoxide in the Asian summer monsoon diagnosed from model of ozone and related tracers (MOZART). *Journal of Geophysical Research-Atmospheres*, 114, D08303.

Qu, X. & Huang, G. (2016) The global warming-induced south Asian high change and its uncertainty. *Journal of Climate*, 29, 2259–2273.

Qu, X., Huang, G., Hu, K.M., Xie, S.P., Du, Y., Zheng, X.T. et al. (2015) Equatorward shift of the south Asian high in response to anthropogenic forcing. *Theoretical and Applied Climatology*, 119, 113–122.

Rao, V.B., Ferreira, C.C., Franchito, S.H. & Ramakrishna, S. (2008) In a changing climate weakening tropical easterly jet induces more violent tropical storms over the North Indian Ocean. *Geophysical Research Letters*, 35, 4.

Sampe, T. & Xie, S.P. (2010) Large-scale dynamics of the Meiyu-Baiu Rainband: environmental forcing by the westerly jet. *Journal of Climate*, 23, 113–134.

Santer, B.D., Wehner, M.F., Wigley, T.M.L., Sausen, R., Meehl, G. A., Taylor, K.E. et al. (2003) Contributions of anthropogenic and natural forcing to recent tropopause height changes. *Science*, 301, 479–483.

Stocker, T.F., Qin, D., Plattner, G.K., Alexander, L.V., Allen, S.K., Bindoff, N.L. et al. (2013) Technical summary. In: Stocker, T.F., Qin, D., Plattner, G.-K., Tignor, M., Allen, S.K., Boschung, J. et al. (Eds.) *Climate change 2013: the physical science basis. Contribution of working group I to the fifth assessment report of the intergovernmental panel on climate change*. Cambridge, United Kingdom and New York, NY, USA: Cambridge University Press.

Wei, W., Zhang, R.H., Wen, M., Kim, B.J. & Nam, J.C. (2015) Interannual variation of the south Asian high and its relation with Indian and east Asian summer monsoon rainfall. *Journal of Climate*, 28, 2623–2634.

Wu, G., Liu, Y., He, B., Bao, Q., Duan, A. & Jin, F.F. (2012) Thermal controls on the Asian summer monsoon. *Scientific Reports*, 2, 404.

Zhang, Q., Wu, G.X. & Qian, Y.F. (2002) The bimodality of the 100 hPa South Asia high and its relationship to the climate anomaly over East Asia in summer. *Journal of the Meteorological Society of Japan*, 80, 733–744.

## SUPPORTING INFORMATION

Additional supporting information may be found in the online version of the article at the publisher's website.

**How to cite this article:** Qu, X., Huang, G., Hou, H., Chen, Z., & Du, Y. (2022). The opposite response of the South Asian high to increasing $CO_2$ at different heights. *Atmospheric Science Letters*, *23*(8), e1093. https://doi.org/10.1002/asl.1093